THE JOURNAL OF BIOLOGICAL CHEMISTRY
Vol. 276, No. 46, Issue of November 16, pp. 43197–43204, 2001

Printed in U.S.A.

A Model of Reversible Inhibitors in the Gastric H^+/K^+-ATPase Binding Site Determined by Rotational Echo Double Resonance NMR*

Received for publication, May 25, 2001, and in revised form, July 26, 2001
Published, JBC Papers in Press, July 30, 2001, DOI 10.1074/jbc.M104808200

Jude A. Watts, Anthony Watts, and David A. Middleton‡§

From the Department of Biochemistry, University of Oxford, South Parks Road, Oxford OX1 3QU, United Kingdom and the ‡Department of Biomolecular Sciences, University of Manchester Institute of Science and Technology, P. O. Box 88, Manchester M60 1QD, United Kingdom

Several close analogues of the noncovalent H^+/K^+-ATPase inhibitor SCH28080 (2-methyl-3-cyanomethyl-8-(phenylmethoxy)imidazo[1,2-*a*]pyridine) have been screened for activity and examined in the pharmacological site of action by solid-state NMR spectroscopy. TMPIP, the 1,2,3-trimethyl analogue of SCH28080, and variants of TMPIP containing fluorine in the phenylmethoxy ring exhibited IC_{50} values for porcine H^+/K^+-ATPase inhibition falling in the sub-10 μM range. Deuterium NMR spectra of a ^2H-labeled inhibitor titrated into H^+/K^+-ATPase membranes revealed that 80–100% of inhibitor was bound to the protein, and K^+-competition ^2H NMR experiments confirmed that the inhibitor lay within the active site. The active binding conformation of the pentafluorophenylmethoxy analogue of TMPIP was determined from ^{13}C–^{19}F dipolar coupling measurements using the cross-polarization magic angle spinning NMR method, REDOR. It was found that the inhibitor adopts an energetically favorable extended conformation falling between fully planar and partially bowed extremes. These findings allowed a model to be proposed for the binding of this inhibitor to H^+/K^+-ATPase based on the results of independent site-directed mutagenesis studies. In the model, the partially bowed inhibitor interacts with Phe^{126} close to the N-terminal membrane spanning helix M1 and residues in the extracellular loop bridging membrane helices M5 and M6 and is flanked by residues in M4.

The P2-type ATPases constitute a family of phosphoenzyme-forming ion pumps that includes the Ca^{2+}-ATPases, Na^+/K^+-ATPases, and H^+/K^+-ATPases (1). All are integral membrane proteins that undergo a series of nucleotide-driven conformational changes to expose binding sites sequentially to ions on each side of the membrane (2). A 2.6-Å crystal structure (3) revealed that the Ca^{2+}-ATPase possesses 10 transmembrane helices (M1–M10), a feature that is believed to be common to this family of proteins. The ATP hydrolysis site and aspartyl phosphorylation site are contained within a major cytoplasmic loop between M5 and M6 (6, 7), and it is thought that cation transport involves binding within an intramembrane domain containing regions M5, M7, and M9 (4, 5).

The gastric H^+/K^+-ATPase (gastric proton pump) is concentrated in parietal cells from where it secretes H^+ into the lumen of gastric glands in electroneutral exchange for extracellular K^+ (8). The assembly consists of a 1035-residue catalytic α-subunit and a 35-kDa glycosylated β-subunit, which plays a role in membrane insertion, organization, and targeting of the protein (9). Catalytic activity of the α-subunit is accompanied by conformational toggling between E_1 and E_1–P, E_2—P, and E_2 forms of the protein. The E_1 forms are responsible for ATP hydrolysis and H^+ binding, and the E_2 forms are associated with K^+ binding, dephosphorylation, and release of H^+ into the lumen (10). Modification of the H^+/K^+-ATPase with the carbodiimide reagent dicyclohexylcarbodiimide revealed that Glu^{857} at the cytosolic face of M7 is an important carboxyl site for cation binding (11). This finding was supported by the results of mutations of Glu^{857} to positively charged residues, which gave a 3-fold reduction in the sensitivity of the H^+/K^+-ATPase to K^+ (12). Mutations in membrane domains M5 and M6 have also indicated that Glu^{820} might play a role in K^+ binding and conformational transitions (13).

Gastric proton pump inhibitors (PPIs)[1] are important probes of the topology and organization of H^+/K^+-ATPase in the membrane as well as valuable pharmaceuticals in the treatment of peptic ulcer disease (14). Many PPIs have been identified, but two have been studied extensively. One is omeprazole, a substituted benzimidazole that reacts covalently with Cys^{813} in the extracellular M5-loop-M6 region of the H^+/K^+-ATPase (15). The other is SCH28080, a substituted imidazo[1,2-*a*]pyridine that binds reversibly and noncovalently to the E_2 and E_2-P forms competitively with respect to K^+ (16), leading to accumulation of the phosphoenzyme and inhibition of ion transport (17). Reversible H^+/K^+-ATPase inhibitors such as SCH28080 have aroused particular interest as potential drugs because their pharmacological activity is modulated by the attendant reduction in gastric acidity after binding to the target protein.

The molecular basis for H^+/K^+-ATPase inhibition by

* This work was supported by a senior research fellowship (to A. W.), a studentship (to J. W.), and equipment awards from the Biotechnology and Biological Sciences Research Council (with the Higher Education Funding Council in England) under the Joint Research Equipment Initiative. The costs of publication of this article were defrayed in part by the payment of page charges. This article must therefore be hereby marked "*advertisement*" in accordance with 18 U.S.C. Section 1734 solely to indicate this fact.

§ To whom correspondence should be addressed. Tel.: 44-161-200-4217; Fax: 44-161-236-0409; E-mail: middleda@bioch.ox.ac.uk.

[1] The abbreviations and trivial names used are: PPI, proton pump inhibitor; DMPIP, 2,3-dimethyl-8-(phenylmethoxy)imidazo[1,2-*a*]pyridinium iodide; TMPIP, 1,2,3-trimethyl-8-(phenylmethoxy)imidazo[1,2-*a*]pyridinium iodide; TM2FPIP, 1,2,3-trimethyl-8-(2-fluorophenylmethoxy)imidazo[1,2-*a*]pyridinium iodide; TM4FPIP, 1,2,3-trimethyl-8-(4-fluorophenylmethoxy)imidazo[1,2-*a*]pyridinium iodide; TMPFIP, 1,2,3-trimethyl-8-(pentafluorophenylmethoxy)imidazo[1,2-*a*]pyridinium iodide; [^{3}H]mDAZIP, 8-[(4-azidophenyl)methoxy]-1-tritiomethyl-2,3-dimethylamidazo[1,2-*a*]pyridinium iodide; omeprazole; CP-MAS, cross-polarization magic angle spinning; REDOR, rotational echo double resonance; GI, gastrointestinal; PIPES, 1,4-piperazinediethanesulfonic acid.

SCH28080 remains unclear. Pre-incubation of the protein with SCH28080 prevents modification of Cys^{813} by omeprazole (18), which implies that there is some overlap in the binding sites of the two inhibitors. Mutation of Glu^{820} to Gln in the extracellular M5-loop-M6 sequence produced an enzyme capable of forming a phosphorylated intermediate with low sensitivity toward K^+ and SCH28080 (13). Swarts and co-workers (20) argued later, however, that this observation reflected the low tendency of the E820Q mutant to adopt the SCH28080-sensitive E_2 form rather than signifying that Glu^{820} plays a direct role in inhibitor binding. Experiments with a photoreactive radiolabeled analogue of SCH28080 ([^{3}H]mDAZIP) showed that two peptide sequences in the N-terminal M1-loop-M2 region reacted with the 4-azidophenyl group of the inhibitor (21). Hence, it has been proposed that SCH28080 and similar inhibitors might interact with the extracellular face of H^+/K^+-ATPase both in the N- and the C-terminal regions (22), a mechanism that appears to underlie the inhibition of Na^+/K^+-ATPase by cardiac glycosides (23).

This model for SCH28080 binding could be tested by determining the molecular conformation of the inhibitor or close analogues when bound to the H^+/K^+-ATPase, thereby placing constraints on the geometry and dimensions of the binding site. Detailed structural information about ATPase inhibitors and other membrane protein ligands has been obtained using high resolution solid-state NMR methods to measure interatomic distances within the molecules at their pharmacological sites of action (24–29). Cross-polarization magic angle spinning (CP-MAS) NMR experiments have been performed previously on a complex between H^+/K^+-ATPase and TMPIP, the non-diazido analogue of mDAZIP (28). The molecular conformation of TMPIP can be expressed in terms of three torsional angles, ϕ_1, ϕ_2, and ϕ_3, which define the relative orientations of the imidazopyridine and phenylmethoxy rings (Fig. 1). The conformation of TMPIP in the binding site was partially determined by calculating torsional angle ϕ_1 (165 ± 15°) indirectly from a measurement of the internuclear distance between ^{13}C labels placed in the N-CH_3 and O-CH_2 groups of the inhibitor (Fig. 1). In the early stages of investigation, however, it was not possible to determine the complete structure of the bound inhibitor unambiguously.

Here, a new strategy has been used to describe the complete active binding conformation of the imidazopyridine class of PPIs. The constraint on torsional angle ϕ_1 determined previously for TMPIP (28) has been combined with new structural measurements on a series of novel and biologically active analogues of TMPIP (TM2FPIP, TM4FPIP, TMPFPIP) containing ^{19}F in the phenylmethoxy ring. The values of torsional angles ϕ_2 and ϕ_3 were probed by measuring dipolar couplings between the N-CH_3 carbon and ^{19}F in the phenyl ring (Fig. 1) using the CP-MAS method rotational echo double resonance (REDOR). The structure of the bound inhibitor and information on the binding site gained from site-directed mutagenesis and photoaffinity labeling were used to describe models for SCH28080 and its analogues at the site of functional efficacy.

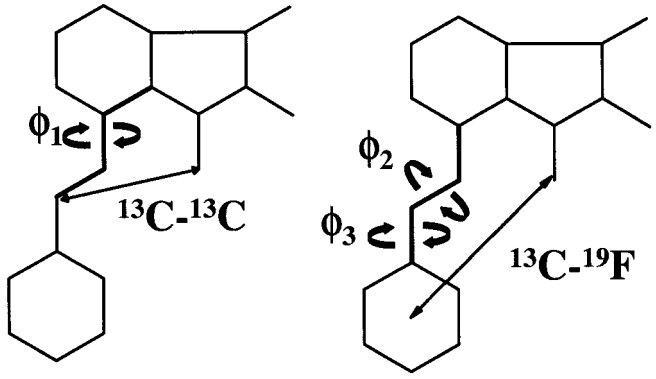

FIG. 1. **Representative structures of 8-phenylmethoxyimidazopyridinium compounds showing the three torsional angles, ϕ_1, ϕ_2, and ϕ_3, which define the complete three-dimensional structure of the molecules.** The structure on the *left* indicates a relationship between the separation of the N-CH_3 and CH_2 groups and angle ϕ_1. Angle ϕ_1 has been measured (165 ± 15°) by rotational resonance NMR (27). The structure on the *right* indicates that the angles ϕ_2 and ϕ_3 are related to distances between the N-CH_3 group and nuclei (in this case ^{19}F) at positions within the aryl ring.

EXPERIMENTAL PROCEDURES

ATPase Preparation and Activity Measurements—Gastric membrane vesicles enriched with H^+/K^+-ATPase were prepared according to a method modified from that previously described (30). Fresh hog stomachs were obtained and transported on ice in a solution of saturated NaCl. The stomach sac was washed of excess mucous, and any remainder was removed by scraping the fundic region with the blunt edge of a knife and with vigorous rubbing with paper toweling. Membrane enrichment was carried out at 4 °C; 60-g batches of crude fundic slices were minced through a press and suspended in Isolation buffer (0.25 M sucrose, 5 mM PIPES, 5 mM Tris-HCl, pH 7.4). The suspension was homogenized using 5 strokes of a mechanical homogenizer operating at ~2000 rpm. The homogenate was separated by ultracentrifugation (Beckman JA-14 rotor, 12,000 rpm, 20 min), and the resulting supernatant was centrifuged to form a pellet (Beckman Ti-45, 40,000 rpm, 45 min). The pellet was resuspended in Isolation buffer and homogenized by 3 strokes of a tight fitting hand-held homogenizer. The suspension was layered over a sucrose/Ficoll density gradient (from the bottom: 15 ml of 30% (w/v) sucrose, 5 mM Tris-HCl, 5 mM PIPES, pH 7.4, 15 ml of 7.5% Ficoll in Isolation buffer) and centrifuged (Beckman SW28 rotor, 24,000 rpm, 90 min). GI microsomal membranes were collected as a band above the Ficoll/Isolation buffer interface. The GI vesicles were maintained by 1:1 dilution in 60% (w/w) sucrose solution (5 mM TRIS-HCl, 5 mM PIPES, pH 7.4) and stored at −20 °C. Protein concentration was determined using a modified Lowry method, and ATPase activity was found according to a method modified from that described elsewhere (31). Lyophilized membranes (10 μg) were added to 0.5 ml of assay medium (2 mM $MgCl_2$·6 H_2O, 2 mM ATP, 20 mM Tris (pH 7.4), 40 mM KCl) and inhibitor. The mixture was incubated at 37 °C for 30 min and quenched by adding 1 ml of ice-cold acid-molybdate (4:1, 5% ammonium molybdate:60% perchloric acid). ATPase activity was estimated as a release of inorganic phosphate from ATP into butyl acetate. K^+-stimulated activity was estimated by subtracting basal activity due to Mg^{2+} stimulation from the activity of the enzyme in the presence of K^+ and Mg^{2+}.

Synthesis of Inhibitors—All of the compounds examined were derived from 2,3-dimethyl-8-hydroxyimidazo[1,2-*a*]pyridine and 2-methyl-8-hydroxy-imidazo[1,2-*a*]pyridine, which were synthesized by methods described previously (32). TM2FPIP, TM4FPIP, and TMPFPIP were prepared in the following manner. 5 mol eq of potassium carbonate in dimethylformamide was added to 1 mol eq of 2,3-dimethyl-8-hydroxyimidazo[1,2-*a*]pyridine. After 30 min of stirring at room temperature, 1 mol eq of 2-fluorobenzylbromide, 4-fluorobenzylbromide, or pentafluorobenzylbromide was added as appropriate, and the reaction was allowed to stir for 48 h during which a scarlet color developed. The reaction was stopped by dropwise neutralization with 1.0 M HCl until the pH was reduced to below pH 7.0. The mixture was filtered and washed with chloroform. The organic phases were pooled and concentrated to give a crimson oil, which was then separated on a Si60 Keiselgel silica column eluting with chloroform:ethyl acetate (4:1). The quaternary ammonium compounds TMPIP (**I**), DMPIP (**II**), TM2FPIP (**III**), TM4PIP (**IV**), and TMPFPIP (**V**) (structures are defined in Table I) were prepared as iodide salts by reaction of the appropriate tertiary amine with 5 mol eq of methyl iodide in 5 ml of acetone. For ^{13}C labeled compounds, ^{13}C-methyl iodide was used in place of the natural isotope abundance reagent. The reaction was stirred under reflux until a precipitate had formed. The reaction was removed from the heat and allowed to cool with stirring. The mixture was filtered, washed with ether, and recrystallized from water.

Inhibition Studies—Substituted imidazo[1,2-*a*]pyridines were dissolved and diluted in ethanol. The final ethanol concentration upon pipetting an aliquot of inhibitor solution was 2% and was regarded as having no effect on the enzyme preparation. The final concentration range of inhibitor assessed in the assay was 0.1 mM--10 nM. All assays were performed in triplicate on three preparations unless otherwise

TABLE I
Summary of the structure-activity relationship of substituted imidazo[1,2-a]pyridines studied in this work

The IC_{50} values represent the half-maximal concentrations for inhibition of K^+-stimulated ATPase activity in purified gastric membranes (GI fraction).

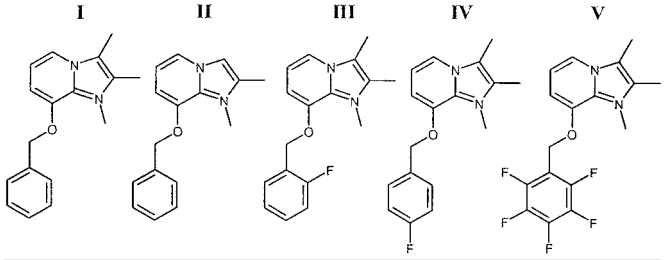

Compound	Name	IC_{50}
		μM
I	TMPIP	2.8 ± 3.5
II	DMPIP	>100
III	TM2FPIP	5.0 ± 0.9
IV	TM4FPIP	2.7 ± 0.7
V	TMPFPIP	8.2 ± 4.0

indicated. The IC_{50} values were defined as the inhibitor concentration that produced 50% inhibition of K^+-stimulated ATPase activity (33). The IC_{50} values were calculated by non-linear least-squares fitting of a sigmoidal function to the experimental data using Microcal™ Origin™ 5.0. The sample size was based on three assays each measured in triplicate for each compound.

Sample Preparation for NMR—Lyophilized H^+/K^+-ATPase membranes (GI fraction) containing 30 mg of protein were prepared as a pellet by centrifugation at 100,000 × *g* for 30 min at 4 °C and incubated with 0–300 μM of labeled inhibitor in 50 μl of incubation medium for 60 min at 37 °C. It was assumed in the first instance that 1 mg of total protein contained 2.5–3.0 nmol of inhibitor binding sites. The pellet was transferred to a 6-mm external diameter zirconia MAS rotor fitted with Kel-F inserts to confine the sample to the center of the rotor.

NMR Experiments—All solid-state NMR experiments were performed on a Varian Infinity spectrometer operating at a magnetic field of 11.7 tesla at temperatures between 5 °C and −50 °C.

Wide-line ^2H NMR experiments were carried out in a probe head fitted with 7-turn 5-mm coil tuned to 76 MHz, using the quadrupole echo sequence with a pulse length of 3.5 μs. CP-MAS experiments were performed by rotating the sample at a MAS frequency (ν_R) of 3–6 kHz. Hartmann-Hahn cross-polarization from ^1H to ^{13}C was achieved over a 1.6-ms contact time at a field of 65 kHz for both nuclei, and protons were decoupled during signal acquisition at a field of 65 kHz. REDOR experiments (^{13}C observe, ^{19}F dephase) were conducted at a sample spinning frequency ν_R of 4500 Hz using a standard pulse sequence with rotor-synchronized π pulses applied at the frequencies of ^{13}C and ^{19}F (34). The π pulse length for both the ^{19}F and ^{13}C frequencies was 9 μs. Numerical simulations of multiple-spin REDOR curves were carried out by adaptation of the general algorithms of Goetz and Schaefer (35).

RESULTS

Inhibition of ATPase Activity—The activities of the five imidazo[1,2-*a*]pyridine analogues TMPIP, DMPIP, TM2FPIP, TM4FPIP, and TMPFPIP were assessed from their concentration-dependent inhibition of ATP hydrolysis by H^+/K^+-ATPase in a lyophilized gastric membrane (GI) preparation (Table I). TMPIP, with an IC_{50} of 3 μM, exhibited a marginally higher (although not statistically significant) activity than the activities of the fluorine-containing analogues. The activities of the fluorinated analogues were in the rank order TM2FPIP = TM4FPIP > TMPFPIP, with TMPFPIP having an IC_{50} of 8.2 μM. By contrast, the analogue DMPIP, which lacks both fluorine and a methyl group at the 3-position of the imidazo ring, was the least active of the compounds studied, exhibiting an IC_{50} of over 100 μM. Hence, the substitution of fluorine into the phenylmethoxy ring has little or no impact on the activity of the inhibitors, whereas minor changes in substitutions to the imidazo ring appear to have a profound effect on activity.

It has been established that an 8-aryl substituent to the imidazopyridine ring system of this class of PPIs is essential for their activity (36), indicating that the aryl group probably plays a key role in the interaction with the binding site. In the compounds examined here, the aryl group was represented either by a phenylmethoxy or fluorophenylmethoxy moiety. The similar activities of these compounds may provide some clues about their binding and inhibitory mechanisms. Fluorine and hydrogen have comparable atomic radii, and replacement of one atom by the other in an aryl group is not expected to alter the steric properties of a molecule. One consequence of substituting fluorine into aromatic rings, however, is to lower the propensity of the aryl π electrons to interact with neighboring cationic groups; the strength of the interaction is reduced progressively as the number of fluorine substituents in the ring increases (37). That the phenylmethoxy and fluorophenylmethoxy compounds have similar activities suggests that the binding mechanism of these inhibitors does not involve an interaction of the phenylmethoxy group with cationic residues in the binding site. It is more probable that the aryl group participates in a π-π stacking interaction with aromatic side groups, because this type of interaction is perturbed much less by fluorine substituents (38).

The close similarity in the activities of TMPIP, TM2FPIP, TM4FPIP, and TMPFPIP indicates that all of these inhibitors share a common binding mechanism, and it is reasonable to assume that the molecular conformation at the binding site is very similar in each case. The torsional angle ϕ_1 of 165 ± 15° determined previously for TMPIP (28) was therefore considered to be a valid constraint in the structural analysis of the fluorine-containing inhibitors.

NMR Characterization of Inhibitor Binding—For reliable determination of the binding conformation of inhibitors it is essential that the inhibitor be observed spectroscopically at its site of action in the H^+/K^+-ATPase. Wide line ^2H NMR was used to investigate the relative proportions of free and bound inhibitor under similar conditions, volumes, and quantities to those used in the REDOR structure analysis (see below). Deuterium was incorporated into the TM2FPIP by forming the quaternary N-CD_3 group in place of N-CH_3 (Table I), and the deuterated inhibitor was titrated into lyophilized GI membranes in molar equivalence to the phosphorylation sites (~3 nmol/mg protein). A representative spectrum of [$^2H_3$]TM2FPIP in gastric membranes (at −5 °C) is shown in Fig. 2*A*. The spectrum exhibits two components in superposition, a narrow central line corresponding to highly mobile inhibitor and a broad powder pattern ascribed to the motion-restricted inhibitor. A comparison of the spectrum with simulated spectra (39) representing different proportions of the two components indicated that the powder component represented over 80% of the total spectral intensity. When [$^2H_3$]TM2FPIP was added to a similarly hydrated volume of extracted gastric membrane lipids, only a single line from the mobile inhibitor was observed (Fig. 2*B*). This indicates that the broad component arose from interaction of the inhibitor with protein in the GI membrane preparation. After the addition of KCl to the GI membranes containing protein-bound [$^2H_3$]TM2FPIP, the broad spectral component disappeared leaving only a single narrow line (Fig. 2*C*). K^+ competes with imidazo[1,2-*a*]pyridines for the same high affinity site on the extracellular face of H^+/K^+-ATPase (16, 17). Hence, these results indicate that over 80% of [$^2H_3$]TM2FPIP added to GI membranes was bound to H^+/K^+-ATPase and could be observed spectroscopically.

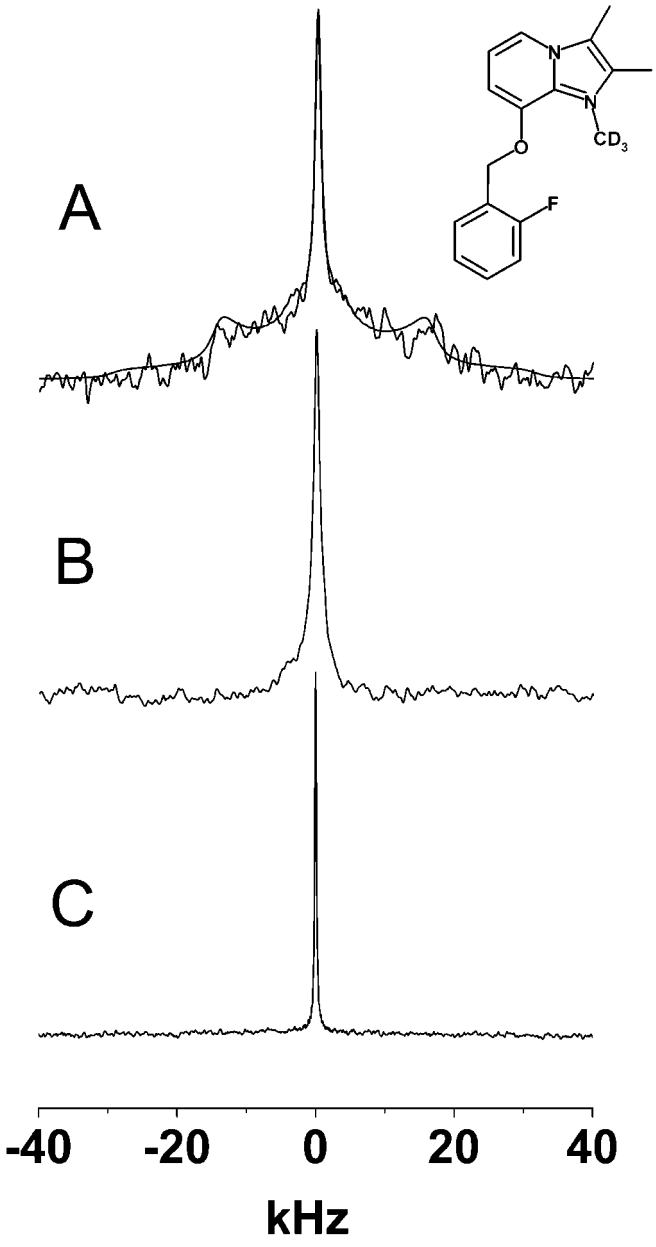

FIG. 2. **Wide line ^2H NMR spectra (at 76 MHz) of [$^2H_3$]TM2FPIP after addition to H^+/K^+-ATPase-enriched gastric membranes.** After titrating the inhibitor into the membranes in approximate molar equivalence to the binding sites, the ^2H NMR spectrum of the membranes showed a broad powder component and a narrow central line (*A*). A similar concentration of inhibitor added to protein-free GI membrane lipids produced only a single narrow line in the spectrum (*B*). The spectrum of [$^2H_3$]TM2FPIP in H^+/K^+-ATPase-enriched membranes also exhibited a single narrow line after dosing the membranes with 0.5 M KCl (*C*). Spectra were recorded at −5 °C, and each spectrum is the result of the accumulation of over 100,000 scans.

Structural Analysis of the ATPase-Inhibitor Complex—The active binding conformation of imidazo[1,2-*a*]pyridines was investigated using the CP-MAS NMR method REDOR (34, 35), which provides interatomic distance information from measurements of dipolar interactions between different atomic nuclei (*e.g.* ^{13}C and ^{19}F). In the REDOR experiment, heteronuclear dipolar couplings, which are usually attenuated or eliminated by magic angle spinning, are reintroduced by applying a train of rotationally synchronous radio frequency pulses at the resonance frequency of one of the nuclear spins (*e.g.* ^{19}F). The signal from the other nuclear spin (*e.g.* ^{13}C) is recorded, and the dipolar coupling constant is measured from the observed dipolar dephased signal intensity after applying the recoupling pulses for a duration defined by the number of sample rotations N_c and the sample spinning frequency ν_R. For a single pair of heteronuclear spins, the internuclear distance is calculated from the quantity S/S_0, which represents the fraction of signal lost (dephased) exclusively as a result of the dipolar coupling between the two nuclei of interest. In practice, the accuracy of the distance measurement is improved by measuring S/S_0 for a range of dephasing times $N_c\nu_R$ (34), although it is possible to measure only at single dephasing times in the case of low sample concentrations (40).

The structures of 8-(fluorophenylmethoxy)imidazo[1,2-*a*]pyridines in the H^+/K^+-ATPase binding site can be probed by REDOR experiments that measure couplings between ^{19}F in the benzyl ring and ^{13}C (the observed nucleus) placed in the N-CH_3 group of the quaternary ammonium cation. In the cases of TM2FPIP and TM4FPIP (Table I, compounds **III** and **IV**) the measured S/S_0 values can be converted directly into single ^{13}C–^{19}F internuclear distances (34), which are, in turn, functions of the relative orientations of the phenylmethoxy group and the imidazopyridine ring. However, numerical simulations of REDOR dephasing curves showed that measurement of a single distance between ^{13}C and ^{19}F at either the 2- or 4-position of the ring cannot provide sufficient information to determine the inhibitor structure unambiguously. The structure could not be resolved from either of these distance measurements even after incorporating the predetermined torsional angle ϕ_1 of 165 ± 15° (28) as a constraint.

To avoid such ambiguities in the structure analysis, we chose to examine the pentafluorophenylmethoxy compound [^{13}C]TMPFPIP (Table I, compound **V**) in the binding site. The presence of five fluorine atoms in the aryl group potentially confers greater sensitivity of the REDOR experiment to molecular conformation, as illustrated by numerical simulations of dephasing shown in Fig. 3. Moreover, the rotational symmetry of the aryl ring eliminates ambiguities associated with the possibility of the fluorine substituent lying *syn* or *anti* to the fused ring system. The combined effect of an ensemble of ^{19}F spins on the ^{13}C signal can be determined for any conformation of TMFPIP by calculating the normalized co-ordinates of the individual spins in a molecular reference frame (35, 41). In practice, values of S/S_0 for any REDOR echo time are computed for many TMPFPIP conformations covering the entire conformational search space, to identify the structure or structures giving the closest fit to the experimental results.

The analysis of the REDOR dephasing of ^{13}C by the five fluorine nuclei in the ring of [^{13}C]TMPFPIP is rather more complex than is the case for a simple spin pair. A complication in the analysis arises from the potential interference of homonuclear coupling between neighboring ^{19}F nuclei in the ring, which attenuates the observed heteronuclear couplings between ^{19}F and ^{13}C (35). In simple cases (*e.g.* homonuclear coupling of two ^{19}F nuclei), it is possible to calculate the extent of attenuation and include compensatory factors in the numerical simulations of REDOR dephasing (42). The structural analysis is more complex for [^{13}C]TMPFPIP because it is difficult to calculate the effect of the network of homonuclear coupling between five ^{19}F nuclei on the REDOR experiment. The simulations of standard REDOR dephasing curves calculated for any given conformation of [^{13}C]TMPFPIP (*e.g.* the *black lines* in Fig. 3) have neglected the effect of ^{19}F–^{19}F coupling and therefore represent the maximum possible dephasing of ^{13}C as a result of heteronuclear coupling to ^{19}F. The actual dephasing for a given conformation (in the presence of ^{19}F–^{19}F coupling) cannot be determined accurately but may fall anywhere between the maximum dephasing and zero dephasing depending

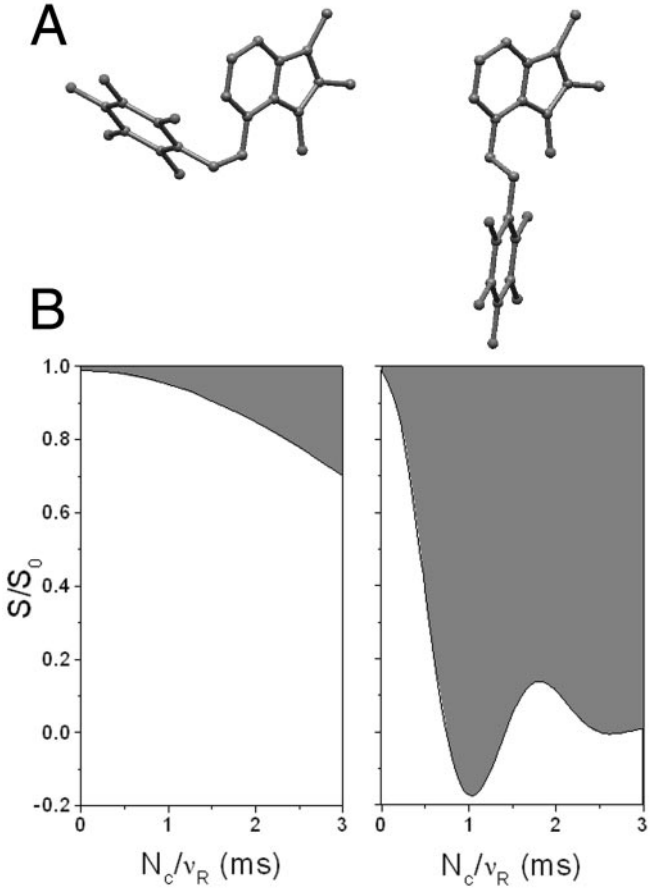

FIG. 3. **An illustration of the relationship between two molecular conformations of [^{13}C]TMPFPIP (*A*) and the predicted response in a ^{13}C observe, ^{19}F dephase REDOR experiment (*B*).** The *dark lines* in the graphs forming the boundary between the gray and white areas show S/S_0 *versus* dephasing time for each of the two molecular conformations as calculated in a molecular reference frame using the algorithms of Goetz and Schaefer (35). The *gray areas* of the graphs signify uncertainties in the dephasing curves arising from nonquantifiable effects of ^{19}F–^{19}F dipolar couplings as described in the text.

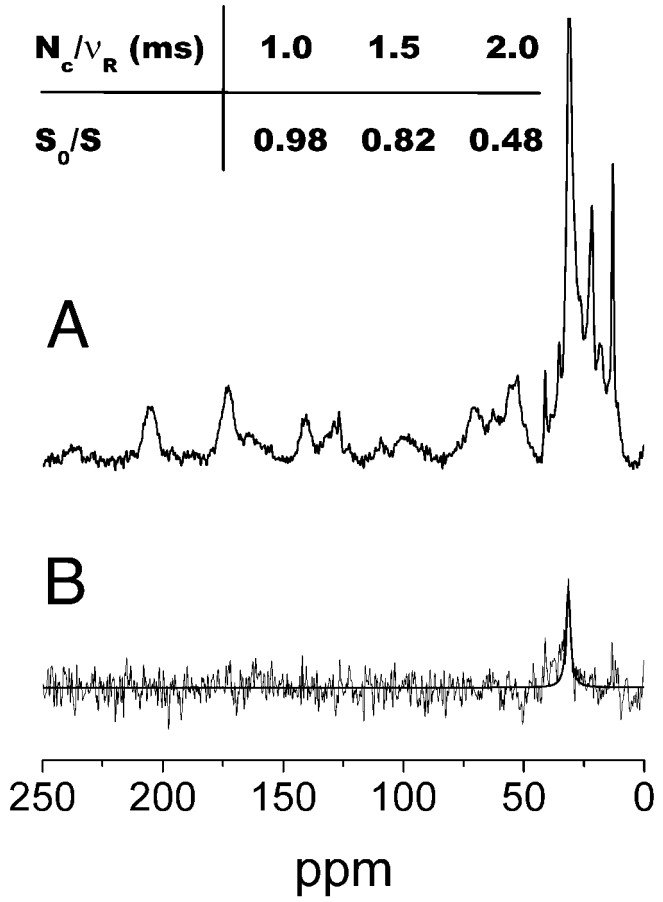

FIG. 4. **The proton decoupled ^{13}C CP-MAS NMR spectrum of GI membranes containing [^{13}C]TMPFPIP (*A*) and a ^{13}C observe, ^{19}F dephase REDOR difference spectrum of the same sample showing the position of the resonance line from the N-$^{13}CH_3$ group of the bound inhibitor (*B*).** The table (*inset*) shows the extent of dephasing (S_0/S) as a function of three dephasing times ($N_c\nu_R$). Spectra were recorded at −50 °C, and the difference spectrum is the result of accumulation of 80,000 scans.

on the interference from ^{19}F–^{19}F coupling. This point is illustrated for the calculated dephasing curves in Fig. 3, in which the *shaded areas* of the graphs above the *solid lines* represent regions of uncertainty in which the dephasing curves may lie when the ^{19}F–^{19}F coupling is non-zero.

The ^{13}C REDOR full echo spectrum of [^{13}C]TMPFPIP bound to H^+/K^+-ATPase in a gastric membrane preparation is shown in Fig. 4. A REDOR difference spectrum obtained by subtraction of the dephased echo spectrum from the full echo spectrum (Fig. 4) shows clearly the ^{19}F dephasing of the ^{13}C resonance line from [^{13}C]TMPFPIP at 32 ppm. The resonance line from the inhibitor therefore lies under the intense peaks from the membrane lipids, and to calculate S/S_0 it was necessary to first remove the interfering natural abundance background signal. This was achieved by subtraction of the corresponding full echo and dephased echo spectra obtained before the addition of inhibitor to the membranes. Using this approach, S/S_0 values were determined for three echo times, 1.0, 1.5, and 2.0 ms (Fig. 4).

The molecular structure of [^{13}C]TMPFPIP in the binding site of H^+/K^+-ATPase was assessed by comparing the observed REDOR dephasing with numerical simulations as described above. Values of S/S_0 at the three echo times were calculated for different combinations of the angles ϕ_1, ϕ_2, and ϕ_3 (Fig. 1) defining the entire conformational space of TMPFPIP. Calculations were based on 5° increments of ϕ_1 from 0 to 180° (the angular constraint determined independently from experiments on TMPIP (28)), 30° increments of ϕ_2 through 360°, and 30° increments of ϕ_3 from 0 to 180° (full rotation was not necessary because of ring symmetry). Hence the conformational analysis covered a search space of 5184 structures. The experimental REDOR data were accepted as being consistent with specific molecular conformations in the search space when the calculated S/S_0 values were greater than or equal to the corresponding experimental values. In this way, the analysis took into consideration the uncertainty in the interference from ^{19}F–^{19}F coupling as described above.

A set of torsional angle combinations was derived from the numerical procedure outlined above, in which each combination of three angles was consistent with the observed REDOR dephasing. The values of ϕ_2 and ϕ_3 covered a small section of the full range, whereas ϕ_1 spanned virtually all values possible (0–180°) and dominated the overall spread of angle combinations. The REDOR approach alone was therefore unable to determine satisfactory constraints for ϕ_1, and hence the value of $\phi_1 = 165 \pm 15°$ determined for TMPIP (28) was introduced as an independent constraint to reduce the spread. This was considered a valid approach because the similar inhibitory behavior of TMPIP and TMPFPIP suggested a common binding conformation of the two inhibitors.

The outcome of the analysis is shown in Fig. 5*A* as points in a three-dimensional graph. Each point on the graph represents a combination of the three torsional angles (*i.e.* a single molec-

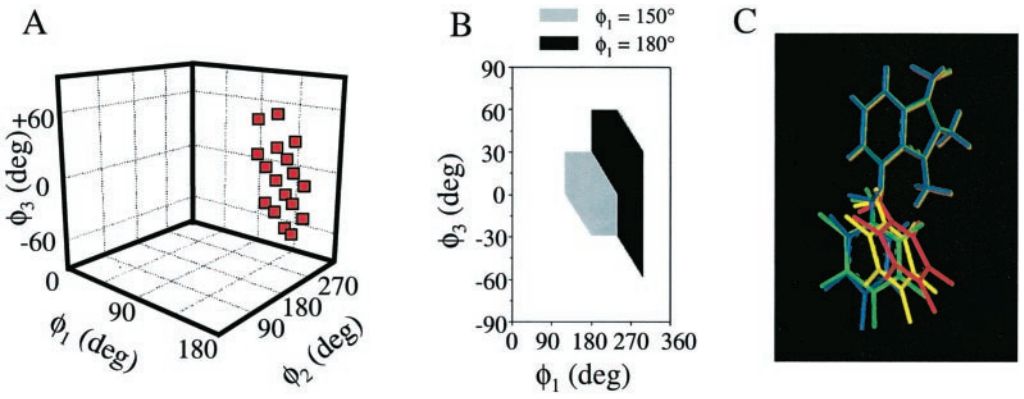

FIG. 5. **Structural analysis of TMPFPIP in the binding site from the REDOR NMR data shown in Fig. 4.** *A*, points on the three-dimensional graph indicate combinations of values of the three torsional angles, ϕ_1, ϕ_2, and ϕ_3 (defined in Fig. 1), which are consistent with the data from rotational resonance (27) and REDOR experiments (refer to "Results" for details of the analysis). *B*, a two-dimensional representation of the torsional angle combinations shows the possible range of angles ϕ_2 and ϕ_3 when angle ϕ_1 is at the upper (180°) and lower (150°) limits of its range of excursion (*black* and *gray* regions, respectively). *C*, the angle combinations translate into an ensemble of TMPFPIP structures, spanning a conformation space in which the true structure lies between planar and slightly bowed extreme.

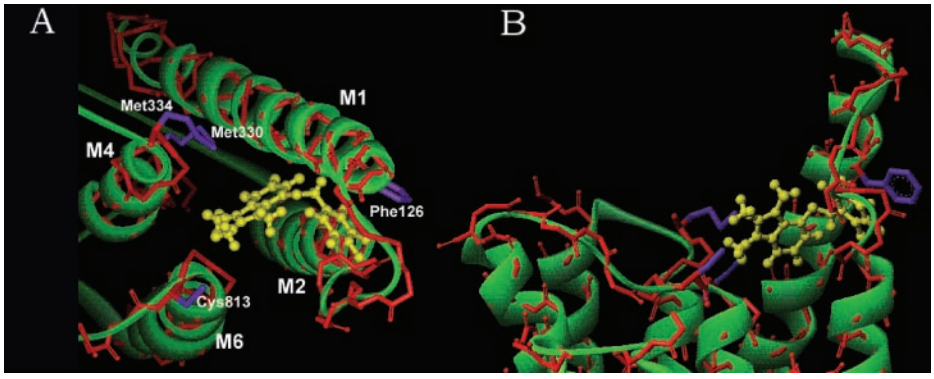

FIG. 6. **A molecular model of TMPFPIP (shown in *yellow*) in the binding site of H^+/K^+-ATPase α-subunit.** An expansion of the proposed M1, M2, M4, and M6 membrane-spanning regions is shown as viewed from above the extracellular face of the membrane (*A*), and an extracellular section of the protein structure is shown as viewed along the plane of the membrane (*B*). The structure and organization of the extracellular and membrane-spanning domains are based on the coordinates of the SERCA1 Ca^{2+}-ATPase crystal structure (3), and the structure of the bound inhibitor was determined by REDOR NMR. In the model, the pentafluorophenyl group of the inhibitor interacts with Phe^{126} in the M1–M2 bridging loop, and the imidazopyridinium cation lies close to Met^{330} and Met^{334} in the M4 transmembrane domain and Cys^{813} in the M5-M6 connecting region. These residues are labeled in *A* and are shown in *purple*.

ular conformation of TMPFPIP) in the search space. By constraining the values of ϕ_1 to within a 30° range, the corresponding angles ϕ_2 and ϕ_3 confined the bound inhibitor to a small cluster of structures. A two-dimensional representation of the angle combinations (Fig. 5*B*) indicates that when $\phi_1 = 180°$, ϕ_2 can take a value within $240 \pm 60°$ and ϕ_3 a value within $0 \pm 60°$ (shown by the *black region* in Fig. 5*B*). When $\phi_1 = 150°$, the spread of ϕ_2 and ϕ_3 (the *gray region* in Fig. 5*B*) is narrower still. A family of TMPFPIP conformations is shown in Fig. 5*C*, which includes conformations lying between the two extreme limits of the search space. At one of the limits the structure is fully planar, and at the other limit the structure shows a slight curvature of the benzyl group relative to the fused ring. All structures in the cluster share a common feature in that the benzyl ring lies extended away from the fuse ring system.

DISCUSSION

There is to date no firm, detailed model for the mechanism of interaction of any class of inhibitor with the H^+/K^+-ATPase. Existing information about the structure of the binding site and the conformational preferences of inhibitors has been obtained in a piecewise fashion using a combination of techniques including site-directed mutagenesis (13) and conventional structure-activity studies (32, 36). Here, solid-state NMR has been used as a complementary technique to provide a direct structural insight into inhibitors at their site of action.

In recent work (29) solid-state NMR measurements were combined with results gained independently from site-directed mutagenesis studies by Lingrel and co-workers (7), to provide a model for cardiac glycosides in the digitalis receptor site of the Na^+/K^+-ATPase. The Ca^{2+}-ATPase structure (3) was used as a framework onto which ouabain-sensitive residues of the Na^+/K^+-ATPase were mapped by sequence threading. The binding conformation of an ouabain analogue was determined by REDOR NMR and docked with the extracellular face of the putative Na^+/K^+-ATPase structure to suggest models for inhibitor binding. Similarly here, the Ca^{2+}-ATPase structure was used as a template of the H^+/K^+-ATPase from which to speculate on the SCH28080 binding site, first taking into account the clear sequential and structural differences between the H^+/K^+-ATPase and the calcium pump.

Photoaffinity labeling experiments using [^{3}H]mDAZIP have suggested that the N-terminal M1–M2 region of the H^+/K^+-ATPase interacts with the 8-aryl substituent (Fig. 1) of SCH28080 and its analogues (21). On the other hand, the results of site-directed mutagenesis suggest that the C-terminal M5–M6 region contains polar or negatively charged side groups that are essential for SCH28080 inhibition (43, 22). Hence, it is possible that the inhibitors are able to extend across the surface of the protein and interact simultaneously with residues in M1–M2 and M5–M6. The spatial relationship

between the inhibitor and the extracellular face of the protein was explored by comparing the binding conformation of TMPFPIP determined by NMR with a model of the H^+/K^+-ATPase based on the Ca^{2+}-ATPase crystal structure (3). The relative dimensions of the inhibitor and the putative arrangement of the H^+/K^+-ATPase transmembrane domains suggests that TMPFPIP is able to span across the membrane surface regions including M1, M2, M4, and M6. The combined results of site-directed mutagenesis experiments were included as additional spatial constraints in the modeling procedure to construct a model for inhibitor binding (Fig. 6). The remaining discussion will describe the features of the model in detail.

Recent mechanistic studies of the pharmacological site for reversible H^+/K^+-ATPase inhibitors have identified a number of residues as candidates for interaction with SCH28080 and its analogues (15, 18–19, 43). From photoaffinity labeling experiments on [^{3}H]mDAZIP, Munson and co-workers (21) suggested that the phenylmethoxy ring of SCH28080 analogues participates in a π-π interaction with Phe^{126} in M1. This argument is supported here by functional studies showing the comparable activity of TMPIP and its fluorophenylmethoxy analogues (Table I). It is unlikely that K^+-competitive inhibitors like [^{3}H]mDAZIP, TMPIP, and SCH28080 bind solely within the M1–M2 region because the K^+ channel region is defined by the M4–M8 transmembrane segments, which lie some distance away from M1 and M2. Moreover, SCH28080 prevents substituted benzimidazoles such as omeprazole from modifying Cys^{813} (18), suggesting that the two classes of inhibitor share a region of interaction in the M5–M6 region.

TMPFPIP was modeled in the binding site by taking Phe^{126} in M1–M2 as a suitable anchor point for the phenylmethoxy ring of the inhibitor around which remote interaction sites for the imidazopyridinium cation could be explored. The extent to which the inhibitor spans the extracellular face of the protein depends on the location of the Phe^{126} side group in the M1-loop-M2 region and its orientation with respect to the body of the H^+/K^+-ATPase α-subunit. If the Phe^{126} ring faces toward the extracellular surface of the protein (Fig. 6), the anchored aryl ring of TMPFPIP allows for the imidazopyridinium ring to interact with M2, M4, and M6 (Fig. 6). Sequence comparison of the H^+/K^+-ATPase M1-loop-M2 region with the first and second transmembrane domains of rabbit skeletal muscle Ca^{2+}-ATPase (3) places Phe^{126} at the position occupied by Ala^{76} in the calcium pump. By analogy with the position of Ala^{76} in the Ca^{2+}-ATPase crystal structure, it is proposed that Phe^{126} lies close to the membrane surface in the extracellular loop just outside the M1 membrane-spanning region, facing toward the body of the protein.

The NMR structure of bound TMPFPIP was compared with the dimensions and arrangement of the H^+/K^+-ATPase extracellular face to assess how far the imidazopyridine moiety of the inhibitor could extend toward the K^+ channel region. REDOR NMR experiments indicated that the active structure of TMPFPIP falls within a small conformational space between fully planar and slightly bow-shaped extremes (Fig. 5). A bow-shaped conformation would allow the imidazopyridine molecule to curve in the interhelical space between the neighboring M1, M2, M4, and M6 transmembrane domains. A simple docking procedure found that the inhibitor could extend away from the Phe^{126} anchor far enough into the body of the protein to allow the imidazopyridinium moiety to interact with residues at the extracellular face of M4 and M6. The M5–M6 region is known to contribute to cation transport, and the reaction of omeprazole with Cys^{813} in this region is blocked in the presence of SCH28080. Moreover, mutation of Cys^{813} to Thr decreases the binding affinity for SCH28080 (22). Hence it is conceivable that the mechanism of action of TMPFPIP and SCH28080 and its analogues involves the inhibitors bridging the intervening space between M1 and M6.

The M6 transmembrane sequence and the extracellular sequence from M5 to M6 were examined to identify polar and negatively charged residues that might interact with the imidazopyridinium ring. From the sequence alignment of Swarts and co-workers (13), the M5 region of H^+/K^+-ATPase terminates at Ser^{806} and is followed by the extracellular bridging loop which re-enters the membrane (as M6) at Ile^{819}. In this model Cys^{813} is exposed to the extracellular environment, which is consistent with the accessibility of this residue to omeprazole and SCH28080. Negatively charged residues that are potentially important for cationic inhibitor binding in the loop-M6 region are Asp^{824} and Glu^{820}, although Glu^{820} is less probable because SCH28080 is able to bind to the phosphorylated E_2P intermediate of the E820Q enzyme mutant (13, 20, 43). Threading the H^+/K^+-ATPase sequence into the Ca^{2+}-ATPase structure places Asp^{824} too far away from M1 to interact with the inhibitor, Glu^{820} in a marginal position for an interaction and Cys^{813} within full reach of the imidazopyridinium cation. Hence, it is suggested that SCH28080 and its analogues interact with Phe^{126} in the M1–M2 extracellular loop and Cys^{813} (or possibly Glu^{820}) in the extracellular loop connecting M5 and M6 (Fig. 6).

One further contribution to this model was taken from the recent work of Munson and co-workers (19), which showed that the binding affinity of SCH28080 is reduced by mutations of residues Met^{330} and Met^{334} in the transmembrane domain M4. By threading the H^+/K^+-ATPase sequence onto the Ca^{2+}-ATPase structure, it is predicted that Met^{330} and Met^{334} are situated just beneath the membrane surface at the sites occupied by Phe^{296} and Val^{300} of the Ca^{2+}-ATPase. A helical wheel view places Met^{330} and Met^{334} facing into the M1–M6 helical space, where they would be available to stabilize the imidazopyridinium cation of SCH28080. It is with some caution that this suggestion is offered, however, because the homology between the two proteins is less satisfactory in the M4 transmembrane region. We have not taken into consideration any evolutionary frameshifts leading to insertions or deletions of amino acids, which would have implications for the orientation of the two methionines in our model.

This work presents the first structure of a reversible inhibitor in the binding site of gastric H^+/K^+-ATPase. It has given valuable insight into the structural requirements for activity of this class of inhibitors and has provided a basis for modeling their interaction with the binding site. Structural information on the H^+/K^+-ATPase is scarce, but it has been possible to suggest a mechanism for inhibitor binding by comparing firm structural data for the inhibitor TMPFPIP with the dimensions of P2-type ATPases. The model proposes that the inhibitor partially spans the extracellular surface of the protein to interact with residues in the first and sixth transmembrane domains. We have made suggestions about the identity of these residues and their approximate location in the protein, but this level of detail remains a matter of speculation until further structural information becomes available.

REFERENCES

1. Stokes, D. L., Taylor, W. R. & Green, M. (1994) *FEBS Lett.* **346,** 32–38
2. Møller, J. V., Juul, B. & le Maire, M. (1996) *Biochim. Biophys. Acta* **1286,** 1–51
3. Toyoshima, C., Nakasako, M., Nomura, H. & Ogawa, H. (2000) *Nature* **405,** 647–655
4. Argüello, J. M. & Lingrel, J. (1995) *J. Biol. Chem.* **270,** 22764–22771
5. Capasso, J. M., Hoving, S., Tal, D. M., Goldshleger, S. J. D. & Karlish, L. (1992) *J. Biol. Chem.* **267,** 1150–1158
6. Lutsenko, S. & Kaplan, J. H. (1995) *Biochemistry* **34,** 15607–15613
7. Lingrel, J. B., Argüello, J. M., Van Huysse, J. & Kuntzweiler TA. (1997) *Ann. N. Y. Acad. Sci.* **834,** 194–206
8. Rabon, E., and Reuben, M. A. (1990) *Annu. Rev. Physiol.* **52,** 321–344

9. Jaunin, P., Horisberger, J. D., Richter, K., Good, P. J. Rossier, B. C. & Geering, K. (1992) *J. Biol. Chem.* **267,** 577–585
10. Wallmark, B., Stewart, H. B., Rabon, E., Saccomani, G. & Sachs, G. (1980) *J. Biol. Chem.* **255,** 5313–5319
11. Rabon, E. C., Hoggatt, M. & Smillie, K. (1996) *J. Biol. Chem.* **271,** 32137–32146
12. Rulli, S. J., Horiba, M. N., Skripnikova, E. & Rabon, E. (1999) *J. Biol. Chem.* **274,** 15245–15250
13. Swarts, H. G. P., Klaassen, C. H. W., de Boer, M., Fransen, J. A. M. & de Pont, J. J. H. H. M. (1996) *J. Biol. Chem.* **271,** 29764–29772
14. Sachs, G & Shin, J. M. (1995) *Annu. Rev. Pharmacol. Toxicol.* **35,** 277–305
15. Besancon, M., Simon, A., Sachs, G. & Shin, J. M. (1997) *J. Biol. Chem.* **272,** 22438–22446
16. Keeling, D. J., Taylor, A. G. & Schudt, C. (1989) *J. Biol. Chem.* **264,** 5545–5551
17. Mendlein, J. & Sachs, G. (1990) *J. Biol. Chem.* **265,** 5030–5036
18. Hersey, S. J., Steiner, L., Mendlein, J., Rabon, E. & Sachs, G. (1988) *Biochim. Biophys. Acta* **956,** 49–57
19. Munson, K. B., Lembrecht, N. & Sachs, G. (2000) *Biochemistry* **39,** 2997–3004
20. Swarts, H. G. P., Hermsen, H. P. H., Koenderink, J. B., Willems, P. H. G. M. & de Pont, J. J. H. H. (1999) *Mol. Pharmacol.* **55,** 541–547
21. Munson, K. B., Gutierrez, C., Balaji, V. N., Ramnarayan, K., and Sachs, G. (1991) *J. Biol. Chem.* **266,** 18976–18988
22. Lambrecht, N., Munson, K., Vagin, O. & Sachs, G. (2000) *J. Biol. Chem.* **275,** 4041–4048
23. Palasis, M., Kutzweiler, T. A., Argüello, J. M. & Lingrel, J. B. (1996) *J. Biol. Chem.* **271,** 14176–14182
24. Watts, A., Burnett, I. J., Glaubitz, C., Middleton, D. A., Spooner, P. J. R., Watts, J. A. & Williamson, P. T. F. (1999) *Nat. Prod. Rep.* **16,** 419–423
25. Watts, A. (1999) *Curr. Opin. Biotechnol.* **10,** 48–53
26. Watts, A. (1999) *Pharmacy Pharmacol. Commun.* **5,** 7–13
27. Williamson, P. T. F., Gröbner, G., Spooner, P. J. R., Miller, K. W. & Watts, A. (1998) *Biochemisty* **37,** 10854–10859
28. Middleton, D. A., Robins, R., Feng, X., Levitt, M. H., Spiers, I. D., Schwalbe, C. & Watts, A. (1997) *FEBS Lett.* **410,** 269–274
29. Middleton, D. A., Rankin, S., Esmann, M. & Watts, A. (2000) *Proc. Natl. Acad. Sci. U. S. A.* **97,** 13602–13607
30. Saccomani, G., Stewart, H. B., Shaw, D., Lewin, M. & Sachs, G. (1977) *Biochim. Biophys. Acta* **465,** 311–330
31. LeBel D., Poirier, G. G. & Beaudouin, A. R. (1978) *Anal. Biochem.* **85,** 86–89
32. Kaminski, J., Bristol, J., Puchalski, C., Lovey, R., Elliott, A., Guzik, H., Solomon, D., Conn, D., Domalski, M., Wong, S-C., Gold, E., Long, J., Chiu, P., Steingberg, M. & McPhail, A. (1985) *J. Med. Chem.* **28,** 876–892
33. Briving, C., Andersson, B-M., Nordberg, P. & Wallmark, B. (1988) *Biochim. Biophys. Acta* **946,** 185–192
34. Pan, Y., Gullion, T. & Schaefer, J. (1990) *J. Magn. Reson.* **90,** 330–340
35. Goetz, J. M. & Schaefer, J. (1997) *J. Magn. Reson.* **127,** 147–154
36. Kaminski, J. J., Wallmark. B., Briving, C. & Andersson, B.-M. (1991) *J. Med. Chem.* **34,** 533–541
37. Ngola, S. M. & Dougherty, D. A. (1998) *J. Org. Chem.* **63,** 4566–4567
38. Williams, J. H. (1993) *Acc. Chem. Res.* **26,** 593–598
39. Zhang, H. & Bryant, R. G. (1997) *Biophys. J.* **72,** 363–372
40. Li, Y, Poliks, B., Cegelski, L., Poliks, M., Gryczynski, Z., Piszczek, G., Jagtap, P. G., Studelska, D. R., Kingston, D. G. I., Schaefer, J. & Bane, S. (2000) *Biochemistry* **31,** 281–291
41. Goetz, J. M., Poliks, B., Studelska, D. R., Fischer, M., Kugelbrey, K., Bacher, A., Cushman, M. & Schaefer, J. (1999) *J. Am. Chem. Soc.* **121,** 7500–7508
42. Espe, M. P., Mattes, B. R. & Schaefer, J. (1997) *Macromolecules* **30,** 6307–6312
43. Asano, S., Matsuda, S., Tega, Y., Shimizu, K., Sakamoto, S. & Takeguchi, N. (1997) *J. Biol. Chem.* **272,** 17668–17674